Orientation Relaxation in Sheared Polystyrene Melts Measured by ^{13}C SMAS-DECODER NMR

Frederick L. Colhoun, Robert C. Armstrong, and Gregory C. Rutledge*

Department of Chemical Engineering, Massachusetts Institute of Technology, Cambridge, Massachusetts 02139

Received March 5, 2001

ABSTRACT: The slow magic angle spinning DECODER NMR technique is used to study the evolution of the orientation distribution function of phenyl rings in polystyrene during stress relaxation following cessation of steady shear flow. Natural abundance ^{13}C is detected in commercial samples of polystyrene sheared at Weissenberg numbers of 33 and 3.3. Moments up to eighth order in a spherical harmonic expansion are used to characterize the steady-state distributions, and the orientational order is observed to decrease as the relaxation proceeds. Contour plots of the orientation distribution function as a function of time are reconstructed from the experimentally determined moments of the distribution. The results emphasize the resolution required to characterize fully the orientation distribution function in deformed polymers.

Introduction

It is widely appreciated that the microstructure of a polymer influences its macroscopic physical properties.[1] Considerable effort has focused on the characterization, on various length scales, of the structural anisotropy of polymers, which manifests itself in anisotropic mechanical and optical properties. Of particular interest is the decay of processing-induced molecular orientation that accompanies stress relaxation in the material, since it directly impacts the amount of frozen-in stress and residual optical birefringence in solid polymers.

Solid-state NMR is a useful tool for studying orientation distributions on the atomic level. Henrichs[2] was the first to develop a 2D exchange NMR technique to measure orientation distributions. Instead of holding the polymer stationary during the mixing time and letting the chains move, he suggested actively flipping the sample during the mixing time, thus reorienting all the chains in the magnetic field. The correlation of frequencies arising from an anisotropic NMR interaction that flips between the two sample orientations in the magnetic field can then be used to deduce the orientation distribution of the associated chemical entity (e.g., chemical shift tensor assigned to a carbonyl group) in the sample. Schmidt-Rohr et al.[3] further developed this concept and coined the term DECODER (direction exchange with correlation for orientation distribution evaluation and reconstruction) NMR. In this case, the correlation of the measured resonant frequencies before and after the mixing time gives information on the orientation distribution of chemical moieties within the sample. Schmidt-Rohr et al. investigated the orientation distributions of uniaxially drawn deuterated polyethylene. Chmelka et al.[4] applied the same technique to the ^{13}C chemical shift anisotropy in biaxially drawn PET. Lewis et al.[5] simplified the implementation of this technique by introducing a slow magic angle spinning (SMAS) version in which the sample is continuously rotated in a standard MAS probe. This eliminated the need for a special reorientation mechanism for the sample during the mixing time, as long as the rotation frequency of the sample is slow relative to the width of the homogeneously broadened chemical shift distribution. The method of Lewis et al. was used by Liao and Rutledge[6] to investigate the molecular orientation in differently processed samples of the HIQ aromatic terpolyester, comprised of 1,4-hydroxybenzoic acid, isophthalic acid, and hydroquinone. A variant of this experiment that measures the dipolar interaction between two neighboring ^{13}C-enriched carbon sites has been used to investigate molecular orientation in polycarbonate deformed plastically in the solid state.[7,8]

Several recent solid-state NMR studies have focused on the characterization of local order in undeformed polystyrene. Robyr et al.[9] investigated order in the packing of phenyl rings in ^{13}C-enriched glassy polystyrene ($M_w = 105\,000$, polydispersity index 1.7) by using a polarization transfer experiment. The data from this study were used to qualify a new computational method for generating realistic chain conformations in polymer glasses.[10] Dunbar et al.[11] studied the correlation of local bond orientations in ^{13}C-enriched polystyrene (M_w unknown) by using a heteronuclear multiple quantum coherence pulse sequence. The distribution of backbone torsion angles was measured, particularly those in the $\bar{g}$ conformation, to test various polystyrene force fields in the literature.

In situ techniques have also been employed to study the orientation of polymer melts during deformation. Apart from the vast amount of literature on birefringence and other optical measurements, the steady-state orientation of polystyrene samples quenched after being subjected to shear flow has been measured by small angle neutron scattering experiments.[12] Furthermore, in situ deuterium NMR techniques have been used to measure the steady-state molecular alignment of PDMS melts in Couette flow through the use of perdeuterated benzene probe molecules.[13,14] The response of polymers to molecular alignment under shear is strongly molecular weight dependent.[15]

The objective of this paper is to reveal the nature of the relaxation of shear induced orientation at a local scale in commercially available polystyrene melts by

* To whom correspondence should be addressed.

10.1021/ma0103932 CCC: $20.00
Published on Web 08/17/2001

Table 1. Relaxation Spectrum for Polystyrene at 165 °C

λ_k (s)	η_k (Pa s)	λ_k (s)	η_k (Pa s)
104.2	135 558	0.122	10 177
10.37	175 955	0.0079	1794
1.068	51 543		

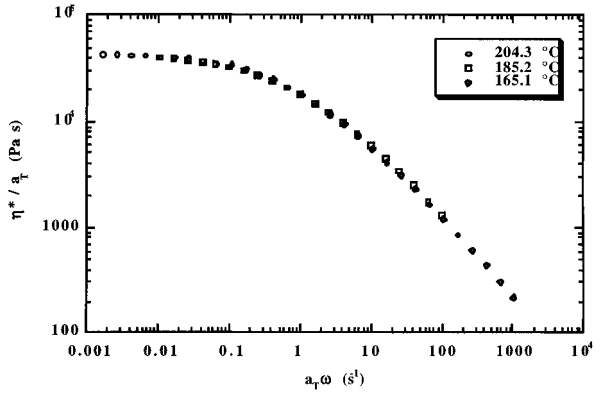

Figure 1. Dynamic viscosity master curve for polystyrene. The reference temperature is 185.2 °C.

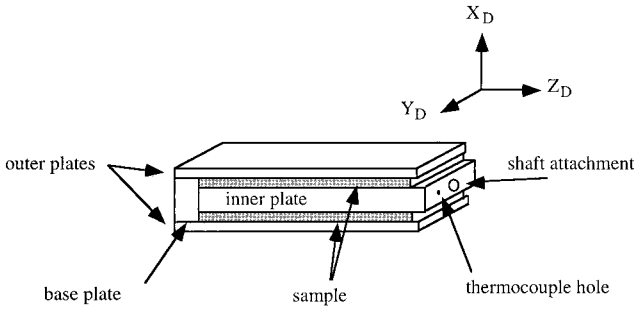

Figure 2. Schematic representation of the interior of the sandwich shear flow cell.

using SMAS-DECODER NMR on samples quenched to below their glass transition at various times during the relaxation process.

Experimental Section

Material. Polystyrene was chosen for this study because of the strong chemical shift anisotropy of the phenyl ring, ease of use and excellent stability of the polymer during melt processing, avoidance of complications associated with crystallization upon cooling, and widespread use of this polymer for rheological studies. The polystyrene used in this study (Huntsman Chemical) was characterized by the manufacturer as "medium flow". The polymer has a weight-averaged molecular weight of 241 000 g/mol and a polydispersity index of 3.0, as determined by GPC. The entanglement molecular weight for polystyrene is 18 100 g/mol.[16]

The longest relaxation time λ_1 for the polystyrene sample used here is 104.2 s at 165 °C. The relaxation time spectrum for the polystyrene, given in Table 1, was determined from a least-squares fit of a generalized Maxwell model[15] to linear viscoelastic data obtained in small-amplitude oscillatory shear flow, shown in Figure 1.

Sandwich Shear Flow Cell Design. A sandwich shear flow cell was constructed on the basis of similar designs for studying uniaxial extensional flow[17] and creep behavior in shear flow.[18] A schematic diagram of the core of the sandwich shear flow cell is shown in Figure 2, along with the definition of the sample frame of reference[6,19] dictated by the deformation geometry. In the multilayer construction, polymer is sandwiched on both sides of the inner plate by the outer plates. The base plate provides the structural support for the entire apparatus. Two end plates, not shown in the figure, cap the flow cell in the neutral direction (Y_D). They are attached to the base plate and have grooves that accept the inner plate. The outer plates are held together by bolts that pass through both outer plates and one of the base or end plates. The deformation is accomplished by pulling the inner plate by means of a worm gear assembly on the drive shaft attached to it.

Penetration theory[20] was used to determine the time required to quench a sample from the melt to the glassy state. For a polystyrene melt at 200 °C, the temperature at a depth of 0.5 mm into the polymer will pass through the glass transition temperature (T_g = 105 °C) 1.8 s after the onset of a thermal quench that uses liquid nitrogen as the heat transfer fluid. A similar penetration analysis was performed to account for the effect of the aluminum outer plate. For a plate thickness of 0.5 mm, the time required for the inner edge of the plate in contact with the polymer to cool to the polystyrene glass transition temperature is 1 ms, 3 orders of magnitude faster than the time required to quench the polymer sample itself. Hence, the 0.5 mm thick aluminum outer plate does not contribute substantially to the quench time for the polymer sample.

For a 0.5 mm thick polymer sample, the dimension in the neutral direction was chosen to be 15 mm. This provided an aspect ratio of 30 and a good approximation to a two-dimensional flow. The sample dimension in the flow direction was then fixed at 30 mm. Although material on both ends of the sample must be trimmed and discarded owing to its no longer being in contact with both the inner and outer plates after the deformation, these dimensions provide enough material on both sides of the inner plate to fill the NMR rotor for shear strains up to 15.

Deformation. The temperature in the sandwich shear flow cell was controlled manually to within 0.3 °C of set point with temporal stability of ±0.2 °C. Upon attainment of steady shear flow in the sandwich device, as estimated from the time required to realize steady-state torque and optical retardance measurements in a separate Couette flow device, the flow was suddenly stopped, and relaxation of the deformed melt was allowed to proceed. Separate samples were obtained by thermally quenching with liquid nitrogen for different time intervals following cessation of the flow. The quenching was performed at constant strain, since the worm gear assembly prevented the inner plate of the sandwich shear device from recoiling.

Flow Cell Sample Preparation. Samples of polymer for use in the sandwich shear flow cell were prepared by using a hot press and a three-layer die. The two outer plates of the die were solid, and the middle plate of the die was 0.5 mm thick and had two 15 mm × 30 mm cutouts. The cutouts were filled with polymer pellets, and the die was heated to 150 °C. The die assembly was then compressed and held at temperature for 2 min, whereupon it was cooled while still under load. The polymer samples were extracted from the die with a razor blade and were inserted into the sandwich shear flow cell without further processing. The samples were held at the operating temperature for at least 1 h prior to deformation to ensure complete relaxation of any molecular orientation generated during the compression of the sample in the hot press.

NMR Sample Preparation. Once the deformation was complete and the samples were vitrified, the outer plates of the sandwich assembly were removed, and the inner plate was pulled away from the samples, which were easily recovered. The samples were then trimmed and split with a razor parallel to the Z_D-X_D plane, taking care to preserve the relative orientation of the resultant strips of material. Material near the edges of the samples was discarded to eliminate edge effects from the deformation. The samples were split to enable the material to fit into the NMR rotor. The strips, each of which was 2 mm × 12 mm × 0.5 mm in size, were stacked and wrapped in Teflon tape (VWR) prior to packing the sample into the NMR rotor. The 12 mm dimension of the strips corresponded to the Z_D axis of the flow cell.

NMR Details. The slow magic angle spinning DECODER NMR experiment was performed on a home-built spectrometer. The static magnetic field strength, as measured by the location

of the proton resonance, was 269.899 MHz. The ^{13}C resonance at this field strength was 67.866 MHz. The carbon and proton 90° pulse lengths were both 5.5 μs. The ^{13}C chemical shift of an external reference standard of TMS was measured as −7812.50 Hz.

The probe was a standard Chemagnetics 7.5 mm double-resonance magic angle spinning probe. The spinning speed ω_r of the rotor was controlled by a Chemagnetics MAS spin controller unit. Feedback control was performed on the optical trigger signal used for the rotor synchronization of the pulse sequence. The spin speed ω_r was either 100 or 200 ±1 Hz over the entire duration of the measurements. A magic angle turning kit (Chemagnetics), which included a restrictor on the drive air line and a special rotor drive tip, was used to achieve the low spin speeds. MacNMR version 5.4 PPC software was used to interface the pulse program and data storage, which were controlled by using the Tecmag LIBRA system.

The details of the SMAS-DECODER pulse sequence have been given elsewhere.[6] The cross-polarization time was 2 ms, and the recycle delay time between repetitions of the pulse sequence was 3 s. In collecting the two-dimensional data sets, dwell times of 20 μs for the 100 Hz spin speed and 10 μs for the 200 Hz spin speed were used in both dimensions. To maintain a constant reorientation angle between the evolution and detection times, the mixing time was varied according to the t_1 increment. Spectra were measured with a varying number of t_1 increments and 256 points during the acquisition. Two hypercomplex data sets were recorded separately and processed with the MacNMR software according to the method described by States et al.[21]

Results and Discussion

Two sets of samples were investigated that were sheared at constant shear rates of $\dot{\gamma}_0 = 0.314$ and 0.0314 s^{-1}, corresponding to Weissenberg numbers $We = \lambda\dot{\gamma}_0$ of 33 and 3.3, respectively, at 165 °C. Nonlinear, elastic effects are expected to be significant at these shear rates.

The material function η^- characterizes the stress relaxation response of a material upon cessation of steady shear flow and is defined by

$$\tau_{yx}(t) = -\eta^-(t,\dot{\gamma}_0)\dot{\gamma}_0 \qquad (1)$$

where

$$\dot{\gamma}_{yx} = \begin{cases} \dot{\gamma}_0 & t < 0 \\ 0 & t \geq 0 \end{cases} \qquad (2)$$

Stress relaxation data for polystyrene at 165 °C, normalized by the viscosity, $\eta^-(t,\dot{\gamma}_0)/\eta(\dot{\gamma}_0)$, are shown in Figure 3. Most of the stress relaxes by 30 s upon cessation of the flow. For $\dot{\gamma}_0 = 0.0314$ s^{-1}, 85% of the stress relaxes by 30 s, whereas 95% of the stress relaxes by 30 s for $\dot{\gamma}_0 = 0.314$ s^{-1}. Therefore, little information was anticipated from samples allowed to relax longer than 30 s prior to quenching. To trace the relaxation of the processing-induced orientation, samples at each shear rate were quenched at 0, 3, 10, and 30 s following cessation of steady shear flow. After the stated period of relaxation, a valve on a tank of liquid nitrogen was opened, and a further 4 s elapsed until the reading of the thermocouple embedded in the inner plate of the flow cell dropped below 100 °C or the interior of the sample cooled to below T_g. This quench time is about twice as long as the theoretical estimate of 1.8 s. The discrepancy is attributed to the time required for the liquid nitrogen to flow between the valve and the flow cell. Some orientation or stress invariably relaxes during the quench period, but not as much as might be inferred from Figure 3, since the relaxation times increase as the temperature decreases during the quench. Processing at higher temperatures was avoided since shorter relaxation times of the material would preclude observation of any significant degree of orientation within 4 s of the cessation of shear. In the subsequent discussion, samples are identified by the Weissenberg number of the steady flow as high (H = 33) or low (L = 3) and the time (0, 3, 10, 30) elapsed between cessation of the flow and thermal quenching (e.g., H30 indicates steady shear flow at a Weissenberg number of 33, followed by 30 s of relaxation prior to quenching).

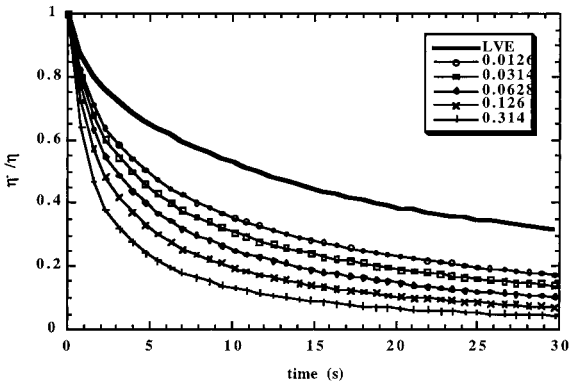

Figure 3. Normalized stress relaxation curves for various initial shear rates at 165 °C. The bold curve represents the linear viscoelastic limit for which the stress relaxation function may be computed analytically from the relaxation time spectrum by $\eta^-(t) = \sum_k \eta_k e^{-t/\lambda_k}$.

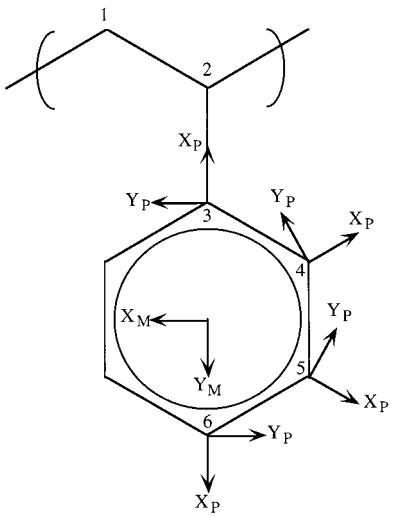

Figure 4. Chemical structure of the polystyrene repeat unit and the definitions of the relevant principal axis systems and the molecular frame of reference.

NMR Analysis. In this paper, the same conventions are used for the relevant reference frames and the angles describing their interconnection as set forth in Liao and Rutledge.[6] The director frame is defined macroscopically by reference to the geometry of the sandwich shear device (Figure 2). The Z_D axis is defined as the flow direction, the X_D axis is defined as the shear gradient direction, and the Y_D axis is defined as the neutral direction of the flow. The principal axis systems associated with each phenyl carbon in the polystyrene repeat unit are illustrated in Figure 4. The values of the chemical shift tensors associated with the principal axis systems used in this analysis were calculated by using quantum chemical techniques.[22] The effect of 180° flips and librational motions of the phenyl rings[23,24] can

Table 2. Principal Values of Polystyrene Phenyl Carbon Chemical Shift Tensors and the Rotation Angles Required To Transform Them into the Molecular Frame

carbon no.[a]	σ_{xx} (ppm)	σ_{yy} (ppm)	σ_{zz} (ppm)	α_p (deg)	β_p (deg)	γ_p (deg)
3	236.0	184.0	18.0	0.0	0.0	90.0
4	237.1	140.0	25.0	0.0	0.0	150.0
5	243.1	149.9	9.9	0.0	0.0	210.0
6	240.6	144.4	7.0	0.0	0.0	270.0
5	243.1	149.9	9.9	0.0	0.0	330.0
4	237.0	140.0	25.0	0.0	0.0	30.0

[a] The carbon labels refer to Figure 4.

be incorporated into the principal values of the chemical shift anisotropies, as described previously.[22] The motionally averaged CSA for each carbon position is shown in Table 2 along with the Euler angles (α_p, β_p, γ_p) necessary to transform the individual principal axis systems into a unified molecular frame of reference. The ring normal is defined as the molecular axis Z_M of the polystyrene repeat unit. The X_M axis lies in the plane of the phenyl ring and is perpendicular to the C2−C3 bond illustrated in Figure 4. Since the phenyl ring is perpendicular to the local chain backbone,[25] the Z_M axis of this molecular frame also corresponds to the local chain direction.

The orientation distribution function of repeat units with respect to the flow geometry, $f(\Psi_M, \Theta_M, \Phi_M)$, was characterized by determining coefficients of an expansion in terms of Wigner rotation matrix elements, D^L_{mn}:

$$f(\Psi_M, \Theta_M, \Phi_M) = \sum_{L=0}^{\infty}\sum_{m=-L}^{L}\sum_{n=-L}^{L} c^L_{mn} D^L_{mn}(\Psi_M, \Theta_M, \Phi_M) \tag{3}$$

The moments of the distribution are related to these coefficients by

$$\langle D^L_{mn}{}^*(\Psi_M, \Theta_M, \Phi_M)\rangle = \frac{8\pi^2}{2L+1} c^L_{mn} \tag{4}$$

where the asterisk denotes the complex conjugate. For all practical purposes, the orientation of the phenyl ring plane, as represented by the X_M axis, is isotropic transverse to the ring normal, which enables reduction of the set of Wigner rotation matrix elements to the set of spherical harmonics ($n = 0$):

$$Y_{Lm}(\Theta_M, \Phi_M) = i^{|m|-m}\sqrt{\frac{2L+1}{4\pi}\frac{(L-|m|)!}{(L+|m|)!}} P^m_L(\cos\Theta_M) e^{-im\Phi_M} \tag{5}$$

where

$$D^L_{m0}(\Psi_M, \Theta_M, \Phi_M) = \sqrt{\frac{4\pi}{2L+1}} Y_{Lm}{}^*(\Theta_M, \Phi_M) \tag{6}$$

Central symmetry[26] of the molecular frame (i.e., $f(\Theta_M, \Phi_M)) = f(\pi - \Theta_M, \Phi_M + \pi)$) allows further contraction to the set of basis functions with L even. Rectilinear shear flow is not invariant to reflection through the Y_D−Z_D plane. Therefore, basis functions with m odd must be included in the analysis. The Z_D−X_D symmetry plane allows the terms containing $\sin(m\Phi_M)$ to be discarded.

The samples were packed into the NMR rotor with Z_D parallel to Z_R. This gives $\theta^n = 0°$ and $\beta_1 = \beta_2 = \theta_m = 54.7°$ (cf. Figure 2 of ref 6). In all cases, the $-X_D$ axis was aligned with the trailing edge of the optical trigger mark on the rotor casing, with the exception of the H0 sample for which the sample was rotated 180° about Z_R. The H0 sample was spun at 100 ±1 Hz, whereas the remaining samples were spun at 200 ±1 Hz over the duration of the experiments due to difficulties encountered in reliably establishing stable spinning at 100 Hz. Spin speeds up to 200 Hz do not affect significantly the acquired spectra because of the large chemical shift anisotropy of the phenyl carbons.[5] These data, combined with a reorientation of 180° during the mixing time, give $\alpha_1 = 326°$ and $\alpha_2 = 146°$ for most of the samples and $\alpha_1 = 73°$ and $\alpha_2 = 253°$ for the H0 sample.

Since the distribution of spectral intensity is dependent on the orientation distribution of the principal axis systems with respect to the magnetic field

$$S(\omega_1, \omega_2) = \int_0^{2\pi}\int_0^{\pi} f(\vartheta, \varphi)\, \delta(\omega_1 - \omega_1(\vartheta, \varphi))\, \delta(\omega_2 - \omega_2(\vartheta, \varphi)) \sin\vartheta\, d\vartheta\, d\varphi \tag{7}$$

it is possible to express the experimental intensity as a basis expansion in subspectra, which are defined by performing the integration in eq 7 by using spherical harmonic basis functions in place of the full orientation distribution function:

$$S(\omega_1, \omega_2) = \sum_{L=0}^{\infty}\sum_{m=-L}^{L}\sum_{n=-L}^{L} c^L_{mn} S^L_{mn}(\omega_1, \omega_2) \tag{8}$$

The angular dependences of the distribution function and the resonant frequencies may be transformed from (ϑ, φ) to $(\Psi_M, \Theta_M, \Phi_M)$ by application of the appropriate rotation matrixes.[6] The coefficients in the basis expansions of eq 3 and eq 8 are identical. The discrete nature of the experimental intensity enables eq 8 to be solved by singular value decomposition. Terms are added successively to the basis expansion until the coefficients $\{c^L_{mn}\}$ and the quality of fit χ^2/σ^2 cease to change within experimental error or until the addition of an additional term causes the resultant distribution function to violate the physical constraint of nonnegativity. In this context,

$$\chi^2 = \frac{1}{N}\sum_{\omega_1,\omega_2} [S(\omega_1, \omega_2) - \sum_{L=0}^{L_{max}}\sum_{m=-L}^{L}\sum_{n=-L}^{L} c^L_{mn} S^L_{mn}(\omega_1, \omega_2)]^2 \tag{9}$$

and σ^2 is the variance in the amplitude of the spectral noise measured in the region of vanishing intensity.

Powder Sample Results. The full SMAS-DECODER NMR spectrum for an isotropic sample of polystyrene pellets, using a 180° sample reorientation about the Z_R axis during the mixing time, is shown in Figure 5. The main features are the strong methylene resonance around 10−70 ppm and the more diffuse set of overlapping signals due to the carbons of the phenyl ring, spanning the spectral region of 0−250 ppm. In the unoriented sample, the phenyl ring signal exhibits a triangular footprint and is symmetric around the $\omega_1 = \omega_2$ diagonal. The signal is relatively weak due to the reliance on natural abundance ^{13}C in commercial polymers. The signal-to-noise ratio in the phenyl region of the spectrum is 11, estimated from the ratio of the maximum intensity in the phenyl region to σ (defined above). The orientation analysis of the polystyrene samples was performed on the frequency interval from

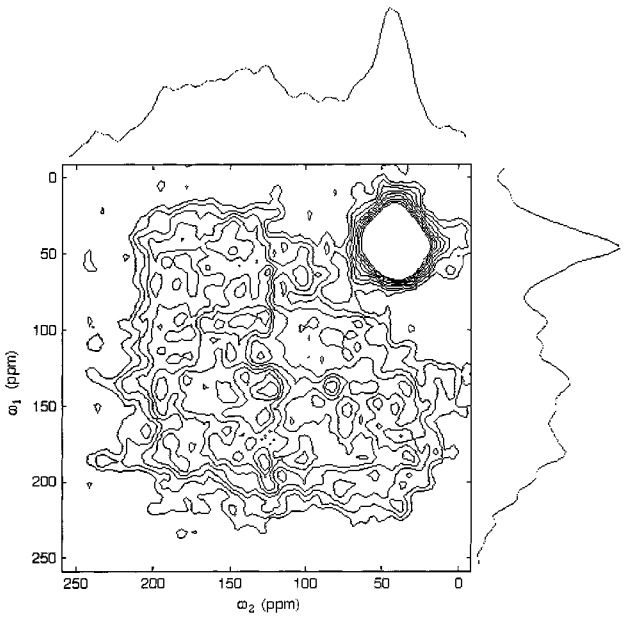

Figure 5. DECODER NMR spectrum for polystyrene pellets with a spin speed of 100 Hz and a reorientation angle of 180° during the mixing time. The contour interval is every 40 from 100 to 420 intensity units.

260 to −10 ppm. Because of the close proximity of the methylene resonance to the phenyl resonance, the spectral region $\omega_1 < 89$ ppm and $\omega_2 < 69$ ppm was excluded from the calculation of the spectral noise and from the linear least-squares matrix problem for the solution of the coefficients of the basis expansion.

The best fit to the experimental spectrum using anisotropic basis functions up to order $L = 2$ (i.e., $Y_{2,0}$ and $Y_{2,1}$) yields moments which are zero within experimental error (0.003 ± 0.010). Inclusion of terms up to order $L = 4$ improves the quality of fit, χ^2/σ^2, from 2.6 to 2.2 and results in significantly nonzero values for the moments $\langle D^4_{0,0}\rangle$ and $\langle D^2_{0,0}\rangle$. This effect can be traced to a drop-off in intensity in the "wings" of the experimental spectrum, $(\omega_1, \omega_2) = (25, 200)$ ppm and (200, 25) ppm, relative to the calculated isotropic spectrum. This feature appears to be common to all of the experimental spectra analyzed in this study. Figure 6 displays the best-fit spectrum for the powder sample using subspectra up to order $L = 4$ for $m = 0$ and 1. The contour interval employed in Figure 6 is half of that used in Figure 5 with the intent of highlighting the intensity ridges in the best-fit spectrum.

To investigate the effect of the CSA tensor principal values on the quality of fit, a sensitivity analysis was performed in which the principal values were varied by ±4 ppm. A separate set of subspectra was calculated using the combination of CSA tensor principal values that minimized χ^2/σ^2. Allowing for inclusion of subspectra up to order $L = 4$ and $m = 1$ resulted in essentially identical values for the best-fit moments obtained using the CSA values of ref 22.

High *We* Results. The DECODER NMR spectrum of the sheared polystyrene H0 sample is shown in Figure 7. The phenyl resonance is peaked at approximately $(\omega_1, \omega_2) = (150, 140)$ ppm. Significant asymmetry is exhibited in the spectral intensity with respect to the $\omega_1 = \omega_2$ line. The intensity is enhanced in the vertical wing (ω_1 dimension) relative to the horizontal wing (ω_2 dimension) emanating from the intensity maximum. The disparity in intensity is particularly noticeable

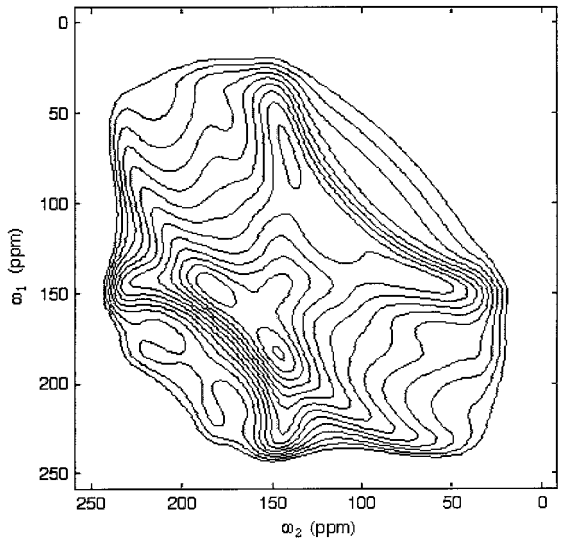

Figure 6. Best-fit reconstruction of polystyrene pellet DECODER spectrum by using a weighted sum of subspectra up to order $L = 4$ for $m = 0$ and order $L = 4$ for $m = 1$. The contour interval is every 20 from 100 to 420 intensity units.

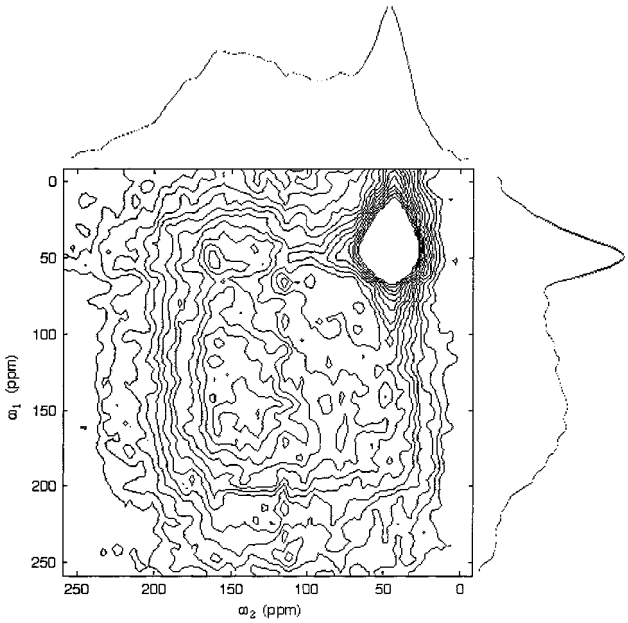

Figure 7. DECODER NMR spectrum of polystyrene H0 sample with a spin speed of 100 Hz and a reorientation angle of 180° during the mixing time. The contour interval is every 100 from 100 to 1500 intensity units.

when comparing the points (150, 50) ppm and (50, 150) ppm. This is indicative of the lack of transverse isotropy of the orientation distribution function of rings with respect to the Z_D axis in these samples. A faint zero frequency pickup artifact is located at $\omega_2 = 115$ ppm. This artifact is more prominent in other polystyrene spectra.

The best fit to the spectrum of the H0 sample is presented in Figure 8 with subspectra up to order $L = 6$ for $m = 0$ and order $L = 4$ for $m = 1$ and $m = 3$. Inclusion of the $Y_{8,0}$ subspectrum led to a worsening of the quality of fit and did not substantially influence the values of the other moments. Inclusion of the $Y_{6,1}$ term, or any terms with $m = 2$ or $m \geq 4$, led to a distribution function with significant negative regions, a result that is aphysical. This was the only sample of the series for which a term with $m = 3$ did not drive parts of the

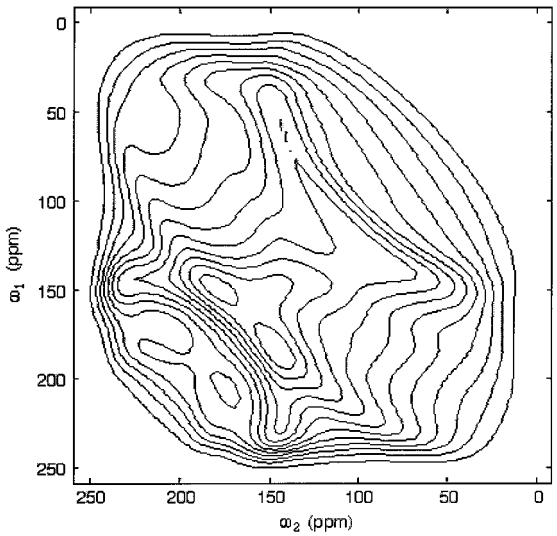

Figure 8. Best-fit reconstruction of polystyrene H0 DECODER spectrum by using a weighted sum of subspectra up to order $L = 6$ for $m = 0$, order $L = 4$ for $m = 1$, and order $L = 4$ for $m = 3$. The contour interval is every 100 from 100 to 1500 intensity units.

distribution function negative. The best-fit value of χ^2/σ^2 is 3.42.The high-intensity ridge in the best-fit spectrum running from (140, 180) to (180, 140) ppm cuts across the edge of the high-intensity peak of the experimental spectrum. The asymmetry of the spectrum is captured by the best fit, as evidenced by the wider vertical ridge compared to the horizontal ridge at 140 ppm in either dimension. The vertical ridge intensity fades at $\omega_1 = 70$ ppm, and the slight peak at $\omega_1 = 50$ ppm in the experimental spectrum is not captured by the best fit. Another significant feature in the best fit spectrum that is not evident in the experimental spectrum is the presence of shoulders at 150 ppm in one dimension, which span from 200 to 230 ppm in the other dimension. These shoulders, or "horns", are characteristic of the isotropic subspectrum. This suggests that the best fit to the experimental data in this case may actually underestimate the amount of orientation present in the sample.

Polar plots of the orientation distribution functions $f(\Theta_M, \Phi_M)$ of the local molecular axis Z_M for samples H0, H3, H10, and H30 are displayed in Figure 9a−d, respectively. These are reconstructed by using the experimentally determined coefficients $\{c^L_{mn}\}$ and eq 3. This set of figures offers a qualitative picture of the evolution of the local chain axis orientation distribution functions during the relaxation process following cessation of steady shear flow at $We = 33$. The Z_D axis, the flow direction, is located at the midpoint of the straight edge of the contour plot. The value of the angle Θ_M is 0° at this point and increases linearly in proportion to cos Θ_M in the radial direction to a value of 90° on the circumference of the plot. The X_D axis, or the shear gradient direction, is located at the top edge of the contour plot. The value of the angle Φ_M is 0° at this point and increases linearly in the azimuthal direction to a value of 180°, representing $-X_D$, at the bottom edge of the contour plot. Thus, the Y_D axis, or the neutral direction, of the sample lies midway around the circumference of the plot. In Figure 9, the distribution functions are positive over the entire domain, normalized, and are plotted with identical contour levels. The darkest contours indicate the lowest values of the orientation distribution function, whereas the lightest contours indicate the highest values of the distribution.

Figure 9a provides the best approximation to the orientation distribution in steady shear flow. The major feature is the peak in the Z_D-X_D plane. This is precisely what is expected in the shear flow of polymers as segments of chains with end points located in different shearing surfaces are rotated toward the flow direction. The peak is offset from the flow direction toward the shear gradient axis. The presence of the peak at positive rather than negative X_D is due to the fact that molecules oriented in the $-X_D$ direction would be rotated rapidly by the flow and would tumble. It is reasonable that the center of the main peak in the distribution function is only slightly above the Z_D-Y_D plane, since at $We = 33$ hydrodynamic forces responsible for chain alignment overwhelm the disordering effect of Brownian forces. The same force balance that causes the peak of the distribution to shift along the positive X_D axis also accounts for the shift in the minimum along the negative X_D axis. Terms of order $L \geq 4$ and $m =$ odd are required to describe this general behavior. However, signal-to-noise considerations limit the number of higher-order terms we can compute reliably. Consequentially, the ring of low probability at $\Theta_M = 45°$ extends over a larger range of Φ_M than we would expect, and we attribute this to truncation of the basis expansion.[27] A larger than expected population of local chain axes are oriented near $\Theta_M = 90°$ for all values of Φ_M. Such perpendicular conformations were observed at low Weissenberg numbers for DNA in shear flow,[28] although the incidence of chains oriented in such a manner decreased with increasing shear rate.[28,29]

Figure 9 shows clearly the changes in the distribution function during relaxation. As the relaxation progresses from 0 to 30 s, the height of the major peak decays and the peak becomes wider, or more diffuse, in Θ_M. During the first 3 s of the relaxation, the location of the distribution function peak shifts from approximately $\Theta_M = 4°$ to $\Theta_M = 11°$, away from the Z_D-Y_D plane, and then more slowly to about $\Theta_M = 13°$ at 30 s.

The evolution of the distribution function during relaxation is expected to be diffusive in nature. The diffusive nature of the structural relaxation is apparent qualitatively, in the broadening of the major peak of the distribution function and in the structural similarity of the distribution functions at different points during the relaxation process. The exception to this observation is the disappearance of the secondary peak in the H0 distribution function at $\Theta_M = 75°$ and $\Phi_M = 130°$. This peak is an artifact that arises from the inclusion of the $Y_{4,3}$ basis function in the H0 fit only. The cos $3\Phi_M$ portion of this basis function gives rise to a peak at $\Phi_M = 120°$, which when combined with the contribution of Φ_M from the $Y_{4,1}$ basis function shifts the peak to $\Phi_M = 130°$. Exclusion of the $Y_{4,3}$ term from the H0 fit results in significantly worse agreement with the experimental data, but inclusion of compensating higher-order terms is precluded by signal-to-noise limitations.

As oriented polymer chains return to their isotropic equilibrium configurations, the probability of finding parts of the chain backbone oriented in any direction should vary with time until the isotropic value is obtained. The persistence of the low probability region in the orientation distribution functions at $\Theta_M = 45°$ and $\Phi_M = 180°$ during the relaxation process suggests that the recovery to isotropic configurations involves a

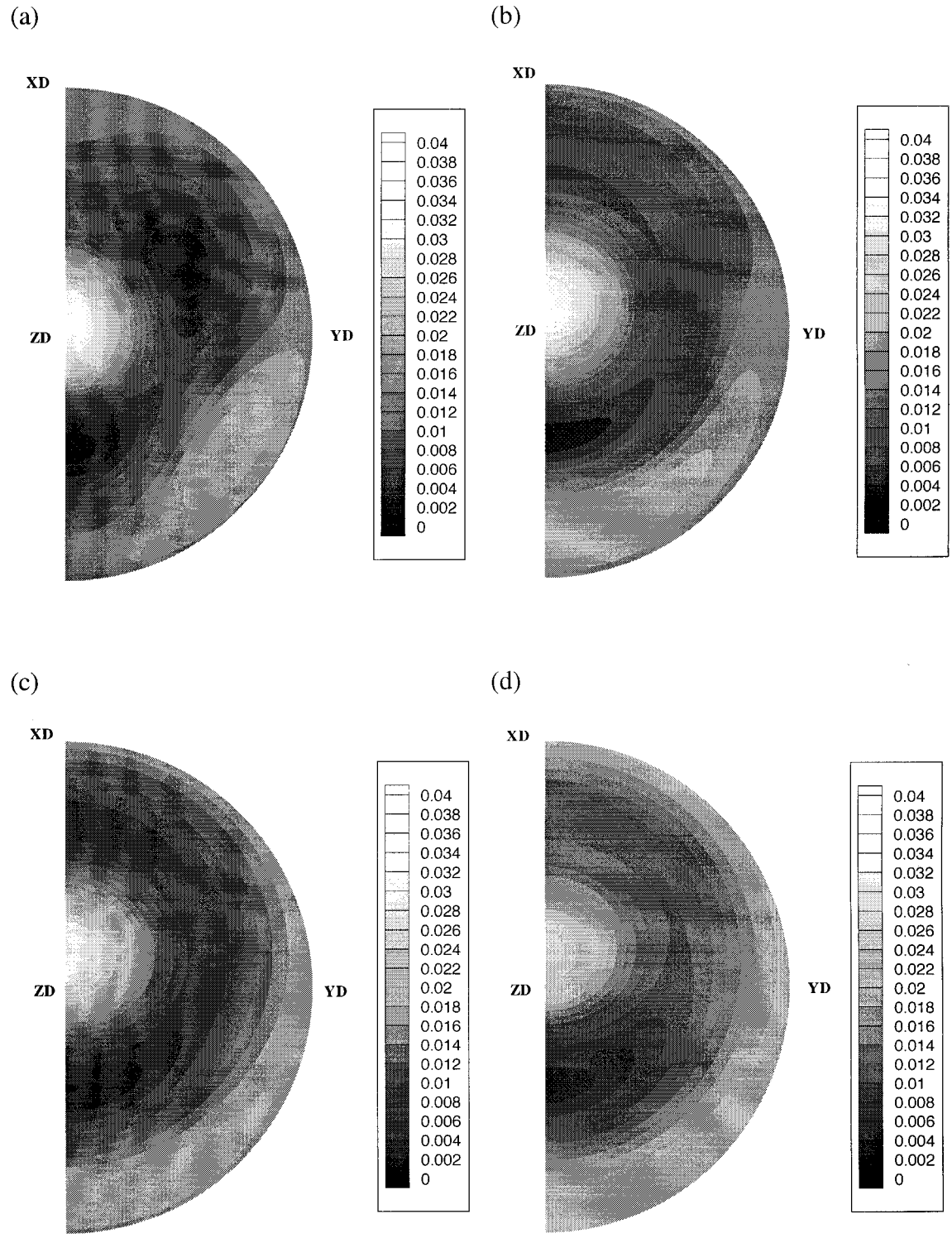

Figure 9. Best-fit orientation distribution functions $f(\Theta_M, \Phi_M)$. (a) H0 sample from spherical harmonic basis functions up to order $L = 6$ for $m = 0$, order $L = 4$ for $m = 1$, and order $L = 4$ for $m = 3$. (b) H3 sample by using spherical harmonic basis functions up to order $L = 8$ for $m = 0$ and order $L = 4$ for $m = 1$. (c) H10 sample by using spherical harmonic basis functions up to order $L = 4$ for $m = 0$ and order $L = 4$ for $m = 1$. (d) H30 sample by using spherical harmonic basis functions up to order $L = 4$ for $m = 0$ and order $L = 4$ for $m = 1$.

second, slower process that occurs well beyond the time scale of 30 s probed by this set of experiments.

Low *We* Results. Figure 10 shows the DECODER NMR spectrum of the L0 sample. The level of detail in this spectrum is not as fine as in the H0 spectrum. This is due to differences in the pulse program required to maintain a constant reorientation angle of 180° during the mixing time. Since the cutoff frequency is twice as large for the L0 spectrum and the same number of data points was acquired, the spectral resolution $\Delta\omega = 5.756$ ppm is half that of the spectra acquired with a rotor spin speed of 100 Hz. The lower resolution spectra exhibited values of σ^2 that were approximately 5 times larger than that in the H0 sample. A particularly severe zero frequency pickup modulation of the spectral intensity is apparent in Figure 10.

The best-fit spectrum with subspectra up to order $L = 6$ for $m = 0$ and $L = 4$ for $m = 1$ is displayed in Figure

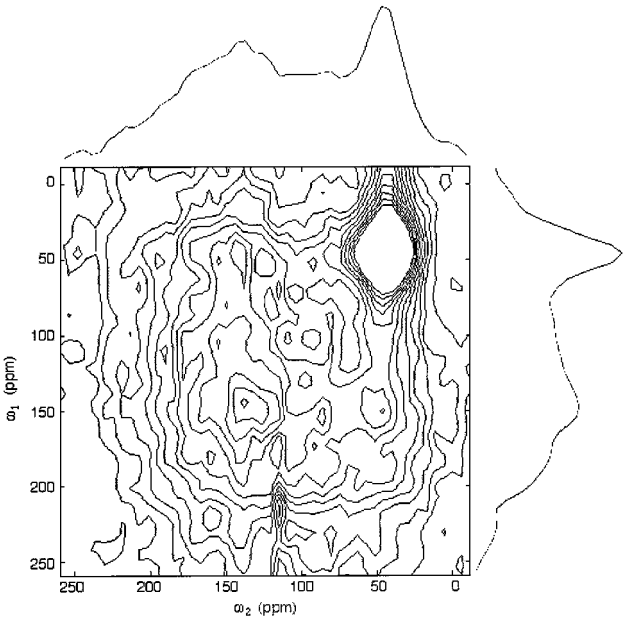

Figure 10. DECODER NMR spectrum of polystyrene L0 sample with a spin speed of 200 Hz and a reorientation angle of 180° during the mixing time. The contour interval is every 150 from 100 to 1600 intensity units.

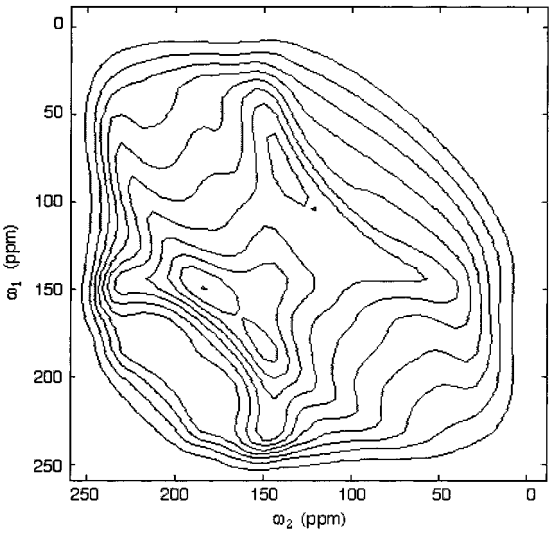

Figure 11. Best-fit reconstruction of polystyrene L0 DECODER spectrum by using a weighted sum of subspectra up to order $L = 6$ for $m = 0$ and order $L = 4$ for $m = 1$. The contour interval is every 150 from 100 to 1600 intensity units.

11. Inclusion of the $Y_{8,0}$ term marginally improved the quality of fit but led to substantially larger error estimates for the lower order moments while not affecting the values of those moments. Inclusion of the $Y_{6,1}$ term worsened the quality of fit. Terms with $m \geq 2$ led to distribution functions with negative regions. The best-fit value of χ^2/σ^2 was 3.02.

The orientation distribution function of the L0 sample is shown in Figure 12 for comparison with the distribution function obtained from the H0 sample. The orientation distribution functions for the other L series samples are not shown, as the form of the distribution functions for the series of samples processed at the lower *We* is identical to that for the samples processed at the higher *We*. Again, the major feature of distribution functions in the L series is the peak in the $Z_D - X_D$ plane at low

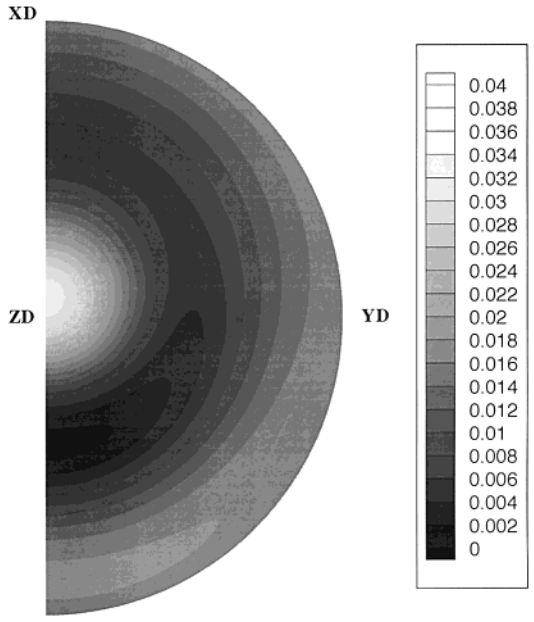

Figure 12. Best-fit orientation distribution function $f(\Theta_M, \Phi_M)$ for L0 sample from spherical harmonic basis functions up to order $L = 6$ for $m = 0$ and order $L = 4$ for $m = 1$.

values of Θ_M. The low probability ring at $\Theta_M = 45°$ is also present.

As in the high *We* experiments, the peak height decreases and the peak becomes more diffuse as the relaxation progresses from 0 to 30 s, and the location of the minimum value of the distribution function remains at $\Theta_M = 45°$ and $\Phi_M = 180°$. The peak height at a given elapsed time during the relaxation is lower for the low *We* samples than for the high *We* samples. This is consistent with the physical reasoning that a weaker flow produces a lesser amount of orientation.

The location of the major peak in the distribution function is about $\Theta_M = 6°$ for the L0 sample, which is slightly farther removed from the flow direction than for the H0 sample. The peak shifts to about $\Theta_M = 11°$ for the L3 sample and remains approximately stationary thereafter. While the shift in the peak location during the first 3 s of relaxation was also observed for the high *We* samples, the peak location continued to migrate slowly in those samples. It is important to note that the migration of the peak during the first 3 s is not due to the structure of the $Y_{4,3}$ basis function used to characterize the H0 distribution, as the effect was also observed in the low *We* samples where this basis function does not arise.

Comparison of Moments. Figure 13 compares the moments of the best-fit orientation distribution functions at various times during the relaxation process. Most apparent is the large magnitude of the fourth-order moments compared to the second-order moments. The large positive $\langle D^4_{0,0} \rangle$ is responsible for the minimum in the distribution functions at $\Theta_M = 45°$, as this coincides with the minimum of that basis function. During the relaxation from steady flow at $We = 33$, the value of the second moment $\langle D^2_{0,0} \rangle$ starts positive and decays to a negative value by 30 s. The value of $\langle D^2_{1,0} \rangle$ begins near zero and decreases steadily over 30 s. The fourth moment $\langle D^4_{0,0} \rangle$ also decays steadily over 30 s and is positive throughout. The other moment common to the fits of all samples, $\langle D^4_{1,0} \rangle$, shows a considerably more complex behavior as a function of time. This is

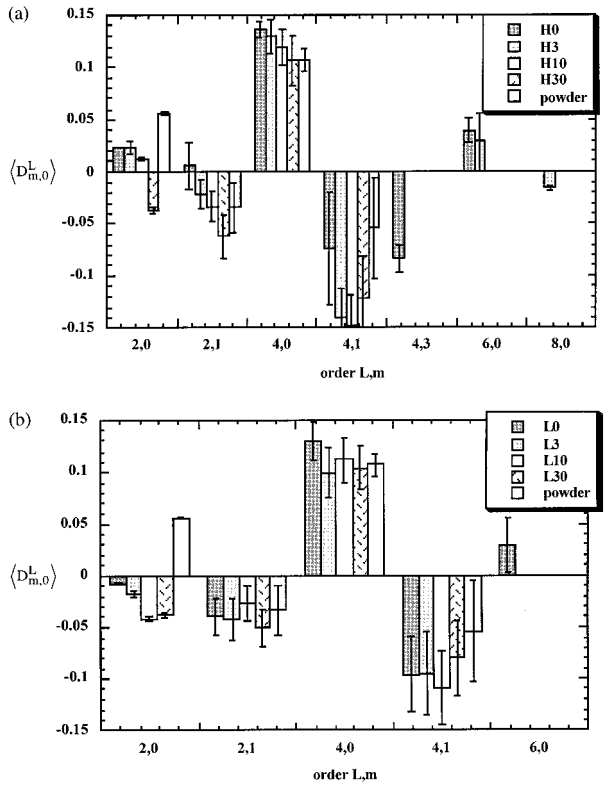

Figure 13. Comparison of the moments of the best-fit orientation distribution functions for the polystyrene samples processed at (a) $We = 33$ and (b) $We = 3.3$. Error bars represent 95% confidence intervals.

the term responsible for isolating the low probability region to $\Phi_M = 180°$. Qualitatively, the decay in the degree of orientation in the samples over a period of 30 s is supported by the loss of higher-order terms ($L \geq 6$ and $m = 3$) in the basis expansions for the H10 and H30 samples. Also, the magnitude of the error estimates tends to increase from the H0 to the H30 sample, indicating that the orientation-dependent component of the spectral signal is becoming more difficult to distinguish from noise as the relaxation process progresses.

For $We = 3.3$, the second moment $\langle D^2_{0,0} \rangle$ becomes increasingly negative as the relaxation progresses. This is in contrast to the high *We* relaxation processes where the second moment is positive for the initial part of the relaxation. It is difficult to detect clear trends in the values of the other moments as the relaxation proceeds, although one may surmise similar trends to those for the high *We* results. Once again, the highest-order basis function $Y_{6,0}$ was only justified in the analysis for the L0 sample, indicating a decay in the degree of orientation as time progressed.

Given the obvious orientational anisotropy exhibited by the sheared polystyrene samples, the low values of the second moment appear surprising. The larger fourth moment in relation to the second moment indicates that the distribution function is more sharply peaked than can be described by the second-order basis functions alone. Also, the offset of the distribution function peak from Z_D, or $\Theta_M = 0°$, does not lend itself to characterization by $P_2(\cos \Theta_M)$ alone. Indeed, the $L \geq 4$ terms are required to capture accurately the offset of the distribution function peak from Z_D.

In both parts of Figure 13, the moments from the fit of the powder sample are displayed for comparison. The significance of the measured anisotropy, as indicated by differences in the moments for the oriented samples from those of the powder sample, is greatest for the H series, particularly at short times. Because of signal-to-noise limitations of this analysis, the local orientation distributions in the L series samples are practically indistinguishable from the isotropic case. This differs substantially from the polycarbonate results in refs 7 and 8 where small, but significant, measures of orientation were detected. In that work, deformation was performed in plane strain compression in the solid state, and the samples used were ^{13}C-enriched. Nevertheless, indications are that a relatively low level of orientation was obtained in those samples. Orientational order (as indicated by the second and fourth moments) in the melt-sheared H-series samples reported here is as much as a factor of 2 greater, and a larger number of higher-order terms in the basis expansion are required to fit the data. However, signal-to-noise limitations limit our ability to fit these higher-order terms reliably.

Conclusions

In this paper, we have presented the first DECODER NMR study of polystyrene. Additionally, we have presented the first attempt by this approach to reveal the manner in which the full orientation distribution function of the local chain axis evolves during stress relaxation of a polymer melt upon cessation of steady shear flow.

Samples were prepared in a sandwich shear flow cell by allowing relaxation to proceed for varying lengths of time before quenching in liquid nitrogen. Analysis of the DECODER spectra of the samples yielded the spherical harmonics moments of the orientation distribution functions. Reconstruction of the distribution function from the moments offers qualitative insight into how the distribution functions change during the relaxation process. The moments of the distributions as a function of relaxation time reflect the decay of orientational anisotropy of the samples.

These results underscore the need for improved data resolution to take full advantage of the method to characterize the orientation distribution functions in deformed polymers. Clearly, methods capable of measuring only up to second- or fourth-order moments cannot characterize important structural features of the orientation distribution functions that may be present. Although theoretically the entire orientation distribution function is accessible in a DECODER NMR analysis, noisy spectra and the enforcement of nonnegativity constraints on the orientation distribution function impose practical limitations on the utility of this method. Some of these problems may be overcome through selection of a more flexible set of basis functions, for example wavelets, or the use of the conjugate orthogonal functions method[30] in the orientational analysis. Expansions in spherical harmonics may be adequate to characterize distributions arising from uniaxial or biaxial extension but require too many terms to describe distributions that are sharply peaked off-axis from the principal deformation directions.

Finally, the ability to measure the orientation distribution functions of repeat units at the level of molecular detail described in this paper offers the possibility of incorporating the data directly into a molecular simulation, thereby modeling a material as it relaxes on the time scale of seconds.[31,32]

Acknowledgment. The authors are grateful to K. K. Gleason and M.-Y. Liao for helpful discussions. This work was funded in part by grants from the 3M Company and by a Young Investigator Award of the National Science Foundation (CTS-9457111).

References and Notes

(1) *Structure and Properties of Oriented Polymers*; Ward, I. M., Ed.; Applied Science: London, 1978.
(2) Henrichs, P. M. *Macromolecules* **1987**, *20*, 2099.
(3) Schmidt-Rohr, K.; Hehn, M.; Schaefer, D.; Spiess, H. W. *J. Chem. Phys.* **1992**, *97*, 2247.
(4) Chmelka, B. F.; Schmidt-Rohr, K.; Spiess, H. W. *Macromolecules* **1993**, *26*, 2282.
(5) Lewis, R. H.; Long, H. W.; Schmidt-Rohr, K.; Spiess, H. W. *J. Magn. Reson.* **1995**, *A115*, 26.
(6) Liao, M.-Y.; Rutledge, G. C. *Macromolecules* **1997**, *30*, 7546.
(7) Utz, M.; Eisenegger, J.; Suter, U. W.; Ernst, R. R. *J. Magn. Reson.* **1997**, *128*, 217.
(8) Utz, M.; Atallah, A. S.; Robyr, P.; Widmann, A. H.; Ernst, R. R.; Suter, U. W. *Macromolecules* **1999**, *32*, 6191.
(9) Robyr, P.; Tomaselli, M.; Grob-Pisano, C.; Meier, B. H.; Ernst, R. R.; Suter, U. W. *Macromolecules* **1995**, *28*, 5320.
(10) Robyr, P.; Muller, M.; Suter, U. W. *Macromolecules* **1999**, *32*, 8681.
(11) Dunbar, M. G.; Sandstrom, D.; Schmidt-Rohr, K. *Macromolecules* **2000**, *33*, 6017.
(12) Muller, R.; Pesce, J. J.; Picot, C. *Macromolecules* **1993**, *26*, 4356.
(13) Callaghan, P. T.; Kilfoil, M. L.; Samulski, E. T. *Phys. Rev. Lett.* **1998**, *81*, 4524.
(14) Kilfoil, M. L.; Callaghan, P. T. *Macromolecules* **2000**, *33*, 6828.
(15) Bird, R. B.; Armstrong, R. C.; Hassager, O. *Dynamics of Polymeric Liquids*, 2nd ed.; John Wiley & Sons: New York, 1987; Vol. 1.
(16) Graessley, W. W. *Adv. Polym. Sci.* **1974**, *16*, 1.
(17) Lundberg, L.; Stenberg, B.; Jansson, J.-F. *Macromolecules* **1996**, *29*, 6256.
(18) Laun, H. M.; Meissner, J. *Rheol. Acta* **1980**, *19*, 60.
(19) Schmidt-Rohr, K.; Spiess, H. W. *Multidimensional Solid-State NMR and Polymers*; Academic Press: New York, 1994.
(20) Deen, W. M. *Analysis of Transport Phenomena*; Oxford University Press: New York, 1998.
(21) States, D. J.; Haberkorn, R. A.; Ruben, D. J. *J. Magn. Reson.* **1982**, *48*, 286.
(22) Colhoun, F. L.; Armstrong, R. C.; Rutledge, G. C. *Polymer*, in press.
(23) Schaefer, J.; Sefcik, M. D.; Stejskal, E. O.; McKay, R. A.; Dixon, W. T.; Cais, R. E. *Macromolecules* **1984**, *17*, 1107.
(24) Spiess, H. W. *Colloid Polym. Sci.* **1983**, *261*, 193.
(25) Rapold, R. F.; Suter, U. W.; Theodorou, D. N. *Macromol. Theory Simul.* **1994**, *3*, 19.
(26) van Gurp, M. *Colloid Polym. Sci.* **1995**, *273*, 607.
(27) Krigbaum, W. R.; Roe, R.-J. *J. Chem. Phys.* **1964**, *41*, 737.
(28) LeDuc, P.; Haber, C.; Bao, G.; Wirtz, D. *Nature* **1999**, *399*, 564.
(29) Smith, D. E.; Babcock, H. P.; Chu, S. *Science* **1999**, *283*, 1724.
(30) Utz, M. *J. Chem. Phys.* **1998**, *109*, 6110.
(31) Rutledge, G. C. *Phys. Rev. E.* **2001**, *62*, 021111.
(32) Colhoun, F. L.; Armstrong, R. C.; Rutledge, G. C. Manuscript in preparation.

MA0103932